Defence Research and Development Canada | Recherche et développement pour la défense Canada

CAN UNCLASSIFIED

DRDC | RDDC
technologysciencetechnologie

Characterizing Transmission Loss Variability During the Target and Reverberation Experiment 2013

Cristina D. S. Tollefsen
Sean P. Pecknold
DRDC – Atlantic Research Centre

IEEE Journal of Oceanic Engineering, Vol. 42, No. 4, pp. 1135–1145

Date of Publication from Ext Publisher: October 2017

Defence Research and Development Canada

External Literature (P)
DRDC-RDDC-2017-P085
October 2017

Canada

IMPORTANT INFORMATIVE STATEMENTS

Characterizing Transmission Loss Variability During the Target and Reverberation Experiment 2013

Cristina D. S. Tollefsen and Sean P. Pecknold

***Abstract*—A significant driver of uncertainty in sonar performance is the variability in underwater acoustical propagation caused by environmental fluctuations and uncertainty in the position of sources, targets, and receivers. A set of echo-repeat experiments was conducted during the Target and Reverberation Experiment 2013 (TREX13), a sea trial that took place in April to May 2013 in the Gulf of Mexico near Panama City, FL, USA. The variability in measured transmission loss (TL) was characterized using two different methods: Variability with respect to a mean observed TL, and variability with respect to modeled TL. Both one-way and quasi-reciprocal two-way TL measurements at 2250 and 7500 Hz were analyzed to characterize the variability at timescales ranging from less than one second to several days, with the results indicating that the acoustic propagation fluctuates stochastically on all these time scales. The results of statistical tests suggest that the TL variability can be treated as Gaussian fluctuations about a central TL obtained from an acoustic propagation model, with standard deviations of 5 dB over timescales up to one day, or 10 dB over timescales from one to six days.**

***Index Terms*—Acoustic propagation, underwater acoustics.**

I. Introduction

THE variability of underwater acoustical propagation has long been recognized as a fundamental problem in predicting sonar performance. Observations of fluctuations in sonar detections during World War II spurred an initial review study on acoustical variability [1] that examined how sound fluctuations could be caused by environmental variability. Since then, variability in the underwater environment and acoustical propagation has continued to be a subject of theoretical and experimental study, particularly in the littoral [2], [3].

Acoustical variability is caused by the effects of environmental fluctuations combined with the uncertainty in position of sources, targets, and receivers. Today, it is impossible to completely determine all aspects of the underwater environment. Therefore, a great deal of work has been undertaken to examine the statistics of environmental and acoustical fluctuations as well as to model the sensitivity of acoustical propagation to uncertain or variable environmental conditions and to determine the effect of this sensitivity on sonar performance predictions [4]–[11].

Manuscript received February 26, 2016; revised January 19, 2017; accepted April 21, 2017. Date of publication May 17, 2017; date of current version October 11, 2017. This work was supported by the U.S. Office of Naval Research, Code 32. *(Corresponding author: Cristina Tollefsen.)*

Guest Editors: B. T. Hefner and D. Tang.

The authors are with the Defence Research and Development Canada, Dartmouth, NS B2Y 3Z7, Canada (e-mail: cristina.tollefsen@drdc-rddc.gc.ca; sean.pecknold@drdc-rddc.gc.ca).

Digital Object Identifier 10.1109/JOE.2017.2699058

In particular, Emerson *et al.* [12] divided variability into short-term and long-term variability, using measurements at 900 Hz in two sites with water depths from 100 to 130 m in the South China Sea. The former is the variability around range-averaged mean TL curves (on the scale of hours), and the latter is the variability of the range-averaged mean curves themselves (greater than 8 h). On the shorter time scales, they found the variability was between 1 and 3 dB, while the long-term (over two years) range-averaged mean TL was not significantly different between the two sites they studied. Previous measurements by Pasewar *et al.* [13] of scintillation index have been made for low frequencies in shallow water (224 and 400 Hz in 54 m of water) and they found that intensities fit more closely to an exponential rather than the lognormal distribution. In addition, Emerson *et al.* [12] and McCammon [14] have considered the question of how inherent uncertainty in propagation and noise impacts detection probabilities.

The goal of this paper is to examine the variability in transmission loss (TL) measured during a set of echo-repeat experiments that took place as part of the Target and Reverberation Experiment 2013 (TREX13) sea trial. The differences in TL variability over space and time, as well as for different waveforms, will be characterized both directly and through the use of propagation modeling.

II. Methods

A. Experiment

1) TREX Experiment Overview: The TREX13 sea trial was a set of underwater acoustical experiments that took place in April to May 2013 in the Gulf of Mexico near Panama City, FL, USA (see Fig. 1). TREX13 was sponsored by the U.S. Office of Naval Research, led by the Applied Physics Laboratory, University of Washington (APL-UW) and Defence Research and Development Canada (DRDC), Dartmouth, NS, Canada. The trial was centered on a fixed source and fixed receiver and a towed echo-repeater deployed in 20 m of water. An extensive set of complementary environmental measurements was designed to facilitate the understanding of the underlying reverberation and clutter mechanisms and support quantitative modeling.

During TREX13 a source and receiver were deployed from the *R/V Hugh R. Sharp*, which was anchored in a four-point mooring. DRDC's research ship, the Canadian Forces Auxiliary Vessel *(CFAV) Quest*, towed an echo-repeat system consisting of a towed receiver, onboard real-time echo-repeat processor,

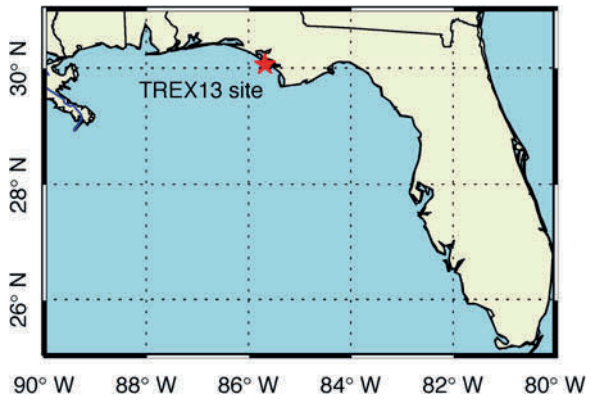

Fig. 1. Location of TREX13 experiment (indicated by a red star) in the Gulf of Mexico.

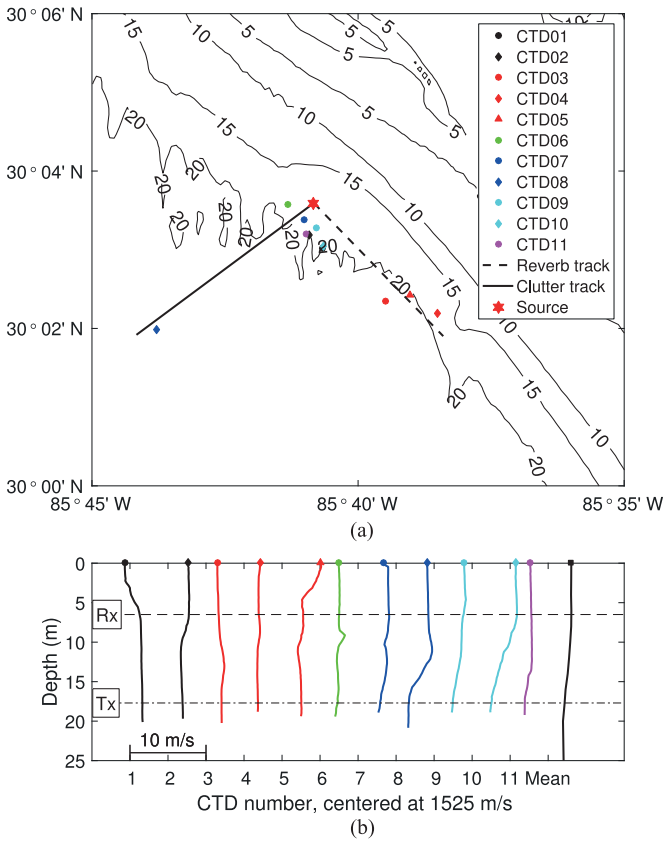

Fig. 2. (a) Echo-repeat run tracks, source location, and CTD measurement locations for May 8–13, 2013, overlaid on bathymetry (m); (b) offset sound-speed profiles from CTD measurements, each centered on 1525 m/s. The mean sound-speed profile was calculated from the 11 measured profiles and extended below the bottom for the purposes of running the propagation model.

and a source to transmit the echo-repeated pulses (see details in Section II-A2 and [15]). The entire series of echo-repeat experiments took place over the period of April 29 to May 13, 2013, and consisted of *CFAV Quest* performing outbound and inbound runs along two tracks relative to the *R/V Sharp* and its colocated source and receiver, one track each in the along-shore and cross-shore directions (see Figs. 2 and 3). The experiment was interrupted several times, including a period of four days due to a storm which forced the *R/V Sharp* to leave its mooring.

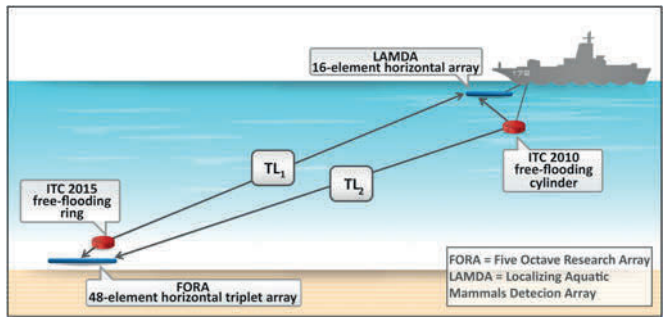

Fig. 3. Schematic diagram (not to scale) of experimental setup (see text for details). A free-flooding ring acoustic source was fixed at a height of 2.1 m above the bottom. *CFAV Quest* towed an echo-repeat system consisting of a line array receiver (6.5-m depth), echo-repeat processor, and free-flooding cylinder source (10-m depth). Echo-repeated transmissions were received on a horizontal line array fixed at 1.2 m above the bottom. Notional direct paths for transmission losses TL_1 and TL_2 are indicated.

TABLE I
EQUIPMENT LOCATIONS FOR ECHO-REPEAT EXPERIMENTS DURING TREX13 (MAY 8–13, 2013)

Equipment	Latitude	Longitude	Note
R/V *Sharp*	30.05990° N	85.68110° W	heading 267°
ITC 2015	30.05975° N	85.68084° W	depth 17.7 m
FORA (center)	30.05927° N	85.68058° W	heading 353°, depth 18.6 m
Reverb track end	30.03170° N	85.06400° W	bearing 129° relative to *R/V Sharp*
Clutter track end	30.03200° N	85.73610° W	bearing 240° relative to *R/V Sharp*

The echo-repeat runs provided a rich data set for analysis and included acoustical effects such as reverberation, bottom loss and scattering, surface loss and scattering, one-way and two-way TL, and target echo [16]. Our main focus is on the TL variability that was observed during these experiments in the period from May 8 to 13, 2013.

2) Echo-Repeat Run Setup: The 17 one-hour echo-repeat runs from May 8 to 13 that are analyzed here were conducted along two tracks, referred to as the reverberation ("reverb") track (along-shore) and the clutter track (cross-shore) (see Fig. 2). Each 10-km long track began at the location of the *R/V Sharp* with its fixed source and receiver (see Table I). Fig. 3 is a schematic diagram (i.e., not to scale) of the overall experimental geometry.

The fixed source was an ITC 2015 free-flooding ring transducer, with an azimuthally symmetric beam pattern and resonance peaks at approximately 2.5 and 7.5 kHz. The source was fixed at a height of 2.1 m above the bottom (17.7 m below the surface).

The incoming transmissions for the echo-repeater were received on a horizontal line array of 16 variably-spaced hydrophones (nominal sensitivity of -185 dB re 1 μPa/V) known as the localizing aquatic mammals detection array (LAMDA array), towed by *CFAV Quest* at a speed of 2.5 m/s. The array was fitted with a pressure sensor to measure the depth, which varied between 4 and 10 m as the ship maneuvered (mean and standard deviation 6.1 $\pm$ 0.8 m). During the straight portion of the runs, the array depth was generally steady near its intended depth of

TABLE II
SOURCE LEVELS BY PING TYPE

Ping name	Length (s)	Description	Source level (dB re 1 μPa at 1 m)	Note
PAS	0.5 s	1800–2700 Hz LFM	197.6	Reduced to 195.0 for dual band runs from May 10 onward
CAS	18 s	1800–2700 Hz LFM	182.1	
Trigger	0.25 s	7000–8000 Hz LFM	199.5	

6.5 m. The incoming transmissions were processed using echo-repeat software developed by DRDC [16], and retransmitted by an ITC 2010 broadband cylindrical transducer that was mounted inside a rigid frame and towed at a notional depth of 10 m (mean and standard deviation 9.6 $\pm$ 0.5 m).

The returned echo-repeat signals were received on the five-octave research array (FORA) [17], a 144-element horizontal triplet array with 0.2-m spacing of the 48 triplets and a sampling rate of 12.5 kHz. The FORA array was tethered in a fixed position near the *R/V Sharp*, 1.2 m above the seafloor (18.6 m below the surface).

In order for the echo-repeater to identify the incoming pulse to be repeated, a 0.25-s trigger pulse consisting of a 7000–8000-Hz linear frequency modulated (LFM) waveform began each transmission, followed by 0.25 s of silence, and then the main echo-repeat waveform. Two main types of waveforms or pulses are discussed here, each with a 20-s repeat rate: Continuous active sonar (CAS) pulses and pulsed active sonar (PAS) pulses. Both were 1800–2700-Hz LFM sweeps, but with two different pulse lengths: 18 s for CAS, and 0.5 s for PAS. Two different modes of echo-repeater were used with both CAS and PAS pulses: The "ping pong" mode and the "dual band" mode, described in more detail in [16]. For the ping pong mode the initial 1800–2700-Hz transmission was recorded and retransmitted during the next incoming pulse (i.e., 20 s later), resulting in echo-repeats for half the pulses. For the dual band mode, two waveforms were transmitted simultaneously: The main 1800–2700-Hz LFM and an out-of-band pulse (3000–4500-Hz LFM) that was 60% as long as the main PAS or CAS pulse. Both pulses were recorded and the out-of-band pulse was echo-repeated at a reduced sample rate 200–500 ms later to emulate the original pulse. All pulses were 10% Tukey shaded (5% at each end). The pulse types and source levels (SLs) used for each are summarized in Table II, while the dates, times, tracks, and pulse types for each run are summarized in Table III. For the "trombone" runs in Table III, *CFAV Quest* began on an outbound track to 5-km range, turned and retraced her path on an inbound track to 3-km range, then turned again and proceeded outbound to 6-km range.

One-way TL was measured using transmissions originating from the fixed ITC 2015 source that were received on the towed LAMDA array for runs between May 8 and 13 (Table III). Comparisons of the quasi-reciprocal ("two-way") TL were also made: The "incoming" transmission loss TL_1 from the ITC 2015 source received on LAMDA was compared with the "outgoing" transmission loss TL_2 from the ITC 2010 source received on FORA. The echo-repeat mode was used on multiple runs with varying target strength settings ranging from 0–25 dB during the May 8–13 period; however, the discussion of two-way TL will be limited to the subset of echo-repeats with 25-dB target strength (r63, r64, r65, r67, r73, and r77, all on May 8 and 9).

TABLE III
SUMMARY OF RUNS (DATES, TIMES, PING TYPES, AND TRACKS) AND CTD CASTS (DATES, TIMES, AND LOCATIONS)

Date/time	Run/CTD	Ping type	Location
May 8, 2013			
08:13 L	CTD01		near source
09:10 L	**r63**	CAS ping pong	clutter outbound
10:30 L	**r64**	CAS dual band	clutter inbound
11:45 L	**r65**	PAS ping pong	clutter outbound
13:00 L	**r66**	PAS dual band	clutter inbound
15:10 L	**r67**	PAS ping pong	reverb outbound
18:43 L	CTD02		near source
May 9, 2013			
04:48 L	CTD03		reverb track end
08:36 L	CTD04		reverb track end
12:00 L	**r73**	CAS ping pong	reverb outbound
16:00 L	**r77**	PAS dual band	reverb outbound
17:56 L	CTD05		reverb track end
May 10, 2013			
07:47 L	CTD06		near source
10:00 L	**r80**	CAS ping pong	clutter outbound
12:00 L	**r82**	PAS ping pong	clutter outbound
14:00 L	**r84**	CAS dual band	reverb outbound
16:00 L	**r86**	PAS dual band	reverb outbound
May 11, 2013			
07:28 L	CTD07		near source
17:51 L	CTD08		clutter track end
May 12, 2013			
07:48 L	CTD09		near source
10:00 L	**r96**	CAS ping pong	reverb outbound
14:00 L	**r100**	CAS dual band	reverb trombone
16:00 L	**r102**	PAS dual band	reverb trombone
18:18 L	CTD10		near source
May 13, 2013			
07:38 L	CTD11		near source
10:00 L	**r106**	CAS dual band	clutter outbound
14:00 L	**r110**	PAS dual band	clutter outbound
15:00 L	**r112**	CAS dual band	reverb outbound

A map of run tracks and CTD locations is provided in Fig. 2.

3) Environmental Measurements: Conductivity-temperature-depth (CTD) casts were performed one to three times each day at locations of convenience (see Table III) as dictated by operational tempo, using a handheld YSI Castaway profiler. Fig. 2(a) is a plot of the locations of CTD casts and the reverb and clutter tracks, overlaid on the local bathymetry. The reverb track approximately follows the 20-m isobath at a heading of 129°, while the clutter track is downslope from the source at a

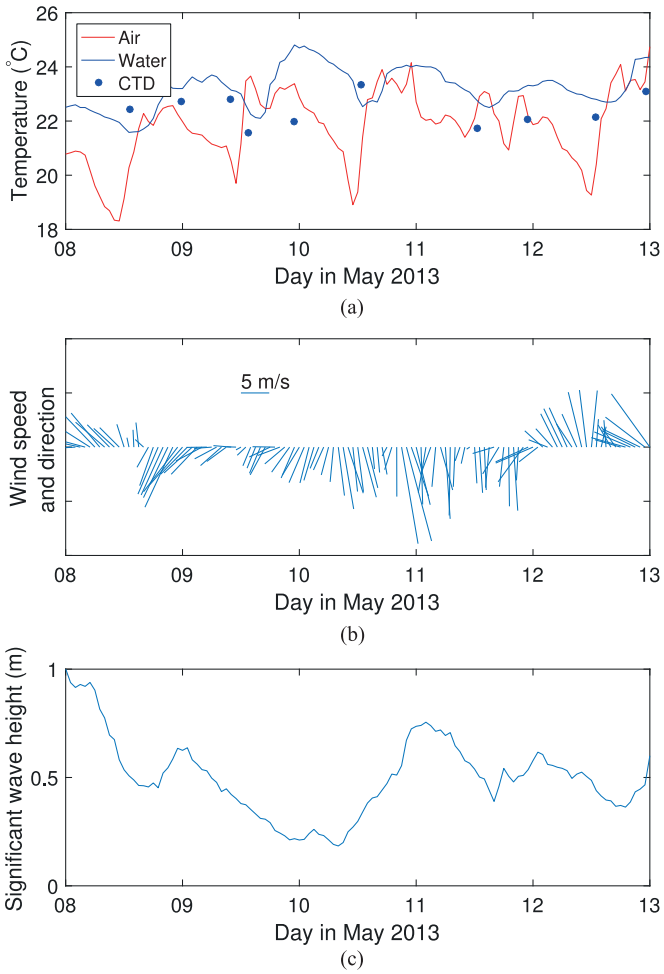

Fig. 4. Environmental conditions at the TREX13 site during the period May 8 to 13, 2013: (a) Air and water temperature from the Panama City tidal gauge station and CTD surface temperature measured by *CFAV Quest*, (b) wind speed and direction as measured by *CFAV Quest*, and (c) significant wave height measured at the TREX13 site.

heading of 240°. The range of water depth along each track is narrow: 18.7–20.5 m for the reverb track, and 18.8–23.9 m for the reverb track.

Fig. 2(b) is a plot of the sound-speed profiles computed from each CTD cast in Table III at the locations in Fig. 2(a). Most of the profiles are weakly downward-refracting at the base of the thermocline, which varies in depth from 8 to 14 m, except for CTD01, which is weakly upward-refracting. The late-afternoon profiles (CTD02, 05, 08, and 10), taken between 17:00 and 18:00 local time, show evidence of a thermocline and stratification caused by solar heating and evaporation during the course of the day. Night-time cooling gives rise to the near-isospeed profiles observed during the night (CTD03) and in the mornings (CTD04, 06, 07, 09, 11).

Fig. 4 provides an overview of the environmental conditions at the trial location during the period of May 8–13 based on hourly averages. Fig. 4(a) is a plot of the air temperature at 5.6-m height and water temperature at 1.5-m depth measured at the Panama City tidal station (Station ID 8729108) as well as the water temperature averaged from surface to 1.5 m measured from the CTD casts (see Table III and Fig. 2). There is a clear diurnal pattern of solar heating for both the air and water temperature, along with an overall increase in water temperatures over the six-day period. Fig. 4(b) is a plot of the wind speed and direction as measured by the anemometers on *CFAV Quest*. On May 8, the wind, originally from the northwest at 5 m/s, shifted direction and reached speeds as high as 8 m/s, remaining between southeast and southwest until May 12, when it again shifted northerly and then northeasterly at speeds of 4–8 m/s. Fig. 4(c) is a plot of the significant wave height measured at the TREX13 site using a Datawell DWR-G4 directional wave buoy at 30.03258°N, 85.64127°W [18]. The correlation coefficient between wave height and wind speed was 0.45, indicating a weak correlation between wind speed and wave height, not surprising since winds from the southerly and southwesterly directions have over 600 km of fetch across the Gulf of Mexico, while those from the north and northeast have very limited fetch given that the TREX13 location was within 15 km of shore.

B. Data Analysis

1) Signal Processing: The TL was computed for each 2250-Hz main pulse (TL_{2250}) and 7500-Hz trigger pulse (TL_{7500}) using matched filter processing. It was not possible to use the integrated energy of the pulse to compute the received level (RL) because the time between the received transmission and echo-repeat transmission (200–500 ms) was less than the pulse length. The bandwidth of the signals allowed sufficient resolution to distinguish the matched filter peaks of the original and echo-repeated pulses.

For the one-way TL calculation from the fixed source to the towed receiver (TL_1), the received signal from LAMDA channel 3 was correlated with doppler-shifted replicas corresponding to relative velocities from -5 to $+5$ m/s. The RL was then given by the maximum of the matched filter output and the TL was computed based on the transmitted waveform SL ($\mathrm{TL} = \mathrm{SL} - \mathrm{RL}$).

For the two-way TL calculation from the towed echo-repeater source to the fixed receiver (TL_2), the RL was calculated by beamforming a linear subarray of 48 hydrophones (the first of each triplet) in the time domain, forming 78 Hanning-weighted beams. A window of ± 2 beams around the bearing from the receiver to the *CFAV Quest* source was used, and the beam time series were matched-filter processed with a set of replicas covering the Doppler space from -10 to $+10$ m/s. Automatic pulse extraction was performed by first calculating local maxima around the expected time-of-arrival using a moving average, and finding the local maximum within 1 s of the expected time-of-arrival. The echo-repeat arrival was then taken as the peak arrival within 0.1 s of that local maximum. The echo-repeat SL was calculated from the voltage applied to the ITC 2010 source modified by its transmitting voltage response curve. The TL was then given by the difference between the SL for the echo-repeated pulse and the peak echo-repeat arrival RL on the fixed receiver ($\mathrm{TL} = \mathrm{SL} - \mathrm{RL}$).

In some cases there were drop outs of either the trigger pulse or of the main pulse and at times the last pulse on some CAS

runs was not fully recorded; therefore these pulses were omitted from further analysis.

2) Third-Octave Range Bin Averaging: For each run, a mean TL curve as a function of range ($\mathrm{TL}_{\mathrm{mean}}$) was computed using a logarithmic range-averaging technique similar to that described by Emerson *et al.* [12]. The TL data were averaged in decibel units at each frequency (2250 and 7500 Hz) using one-third octave range bins centered on 500–10 000 m. In addition, mean TL curves for each track were calculated by combining data from all runs on the same track, and an overall mean TL curve for the entire data set was calculated by combining data from all the runs.

3) Model Setup: TL modeling was performed using DRDC's implementation of the Bellhop model [14], [19]. The model was run in incoherent mode at 2250 and 7500 Hz, with a 10-m range step and 0.5-m depth resolution. Other model inputs included the range-dependent bathymetry as measured by *CFAV Quest* along the clutter and reverb tracks, a sound-speed profile, and a wind speed. Since all the CTD casts (see Table III) were temporally or spatially separated from the echo-repeat runs, and given the timescale of changes to the water column, it was not clear what the "closest" CTD cast would be for each run; therefore, the mean sound-speed profile over the six-day period from May 8 to 13 [plotted in Fig. 2(b)] was used as a model input. The mean wind speed during the same period was used along with the Beckmann–Spizzichino surface scattering submodel in Bellhop. Based on results from *in situ* measurements taken during the trial using a free-fall cone penetrometer, the bottom was modeled as a semi-infinite fluid layer with sound speed $c_b = 1660$ m/s, density $\rho_b = 1.9$ kg/m^3, and attenuation $\lambda_b = 0.5$ dB/λ.

To validate the use of the narrowband model at each center frequency, a broadband coherent TL model [20] was run using the mean sound-speed profile, and the output was averaged over range and depth bins corresponding to the CAS and PAS signals. The mean and standard deviation of the difference between the narrowband and broadband models was 0 ± 2 dB.

4) Variability Analysis: The goal of this paper is to characterize TL variability about a "central" TL and to determine whether the variability is normally distributed about the central TL. It is not immediately clear how to determine a suitable central TL when the TL varies on so many different time and spatial scales; therefore, two choices for central TL were investigated: The mean observed TL (Section II-B2), and TL derived from a model (Section II-B3). To approximately match their time and spatial scales, the mean TL for each track was used, and the modeled TL was based on the overall mean sound-speed profile and the corresponding bathymetry for each track.

The variability with respect to the mean TL was computed for each pulse as the difference between the measured TL (TL_{2250} or TL_{7500}) and $\mathrm{TL}_{\mathrm{mean}}$, which was linearly interpolated in range from the range-averaged $\mathrm{TL}_{\mathrm{mean}}$ curve for the same ship track and frequency, giving $\Delta\mathrm{TL}^{2250}_{\mathrm{mean}} = \mathrm{TL}_{2250} - \mathrm{TL}_{\mathrm{mean}}$ and $\Delta\mathrm{TL}^{7500}_{\mathrm{mean}} = \mathrm{TL}_{7500} - \mathrm{TL}_{\mathrm{mean}}$[12], [21].

The variability with respect to the modeled TL was computed for each pulse as the difference between the measured TL and modeled TL at the same range and depth for the same ship track and frequency, resulting in $\Delta\mathrm{TL}^{2250}_{\mathrm{model}} = \mathrm{TL}_{2250} - \mathrm{TL}_{\mathrm{model}}$ and $\Delta\mathrm{TL}^{7500}_{\mathrm{model}} = \mathrm{TL}_{7500} - \mathrm{TL}_{\mathrm{model}}$. Although there was a record of receiver depth at each pulse time, preliminary testing revealed that the array did not always lie horizontally while under tow, and it was subject to significant changes in tilt and depth (e.g., 2-m depth change in 20 s) during course corrections as small as 15°. Therefore, the uncertainty in receiver depth for a given pulse was taken into account by determining the range of depths during the previous pulse, current pulse, and following pulse, and then calculating a depth-averaged $\mathrm{TL}_{\mathrm{model}}$ as a function of range over this depth window. Next, $\mathrm{TL}_{\mathrm{model}}$ was calculated by either interpolating in range (for pulses less than 1-s long), or averaging over range traveled by the ship during the pulse (for pulses longer than 1 s).

5) Statistical Tests: Two statistical tests were applied to various groupings of the Δ_{TL} data: The Anderson–Darling (AD) test to determine whether data were normally distributed, and the two-sample Kolmogorov–Smirnov (KS) test to determine whether different data sets were drawn from the same underlying distribution. For all the statistical tests described in Section III, the level of significance used to reject the null hypothesis was $\alpha = 0.001$.

The AD test for normality [22] was used to determine whether distributions of variability $\Delta\mathrm{TL}$ within a run fit a Gaussian distribution with unknown parameters [23]. The AD tests produces a test statistic and an associated p-value, which expresses the probability of obtaining a test statistic at least as large if indeed the null hypothesis is correct. The null hypothesis H_0 for the AD test is that the data are normally distributed; p-values less than the chosen level of significance α were used as evidence to reject the null hypothesis.

The two-sample KS test was used in two ways: 1) On each run with the pair of sets of $\Delta\mathrm{TL}$ at the two frequencies; and 2) on pairs of sets of $\Delta\mathrm{TL}$ at the same frequencies from different runs. The KS test compares the cumulative distribution function of two data sets under the null hypothesis H_0 that the sets are sampled from sets of identically distributed data [24], [25]. The p-value associated with each KS test indicates the probability that the value of the statistic would be exceeded under the null hypothesis, i.e., if the observed p-value is lower than a predetermined level of significance α the null hypothesis is rejected and the two sample sets are assumed to be drawn from different distributions.

III. Results and Discussion

A. Model Results

An example of the TL model results is shown in Fig. 5, which is a false-color image of the modeled TL as a function of range and depth along the reverb track at 2250 Hz [see Fig. 5(a)] and 7500 Hz [see Fig. 5(b)]. Fig. 5(c) is a plot of the TL at the nominal receiver depth (6.5 m) as a function of range. There are significant differences in the spatial pattern and values of the TL for the two frequencies: In Fig. 5(c) the TL at the receiver depth (dashed black line) is 75 dB at 10-km range and 2250 Hz and 90 dB at the same range and 7500 Hz.

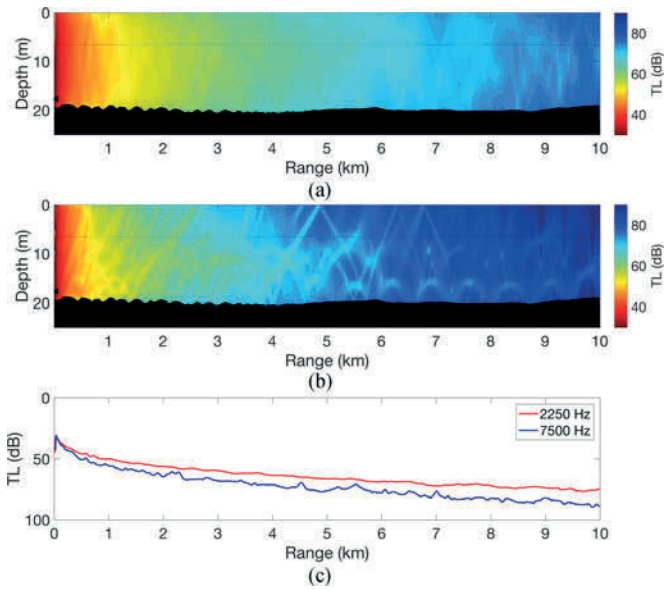

Fig. 5. False-color images of modeled incoherent TL (dB) as a function of range (km) and depth (m) along the reverb track, using the mean sound-speed profile (a) at 2250 Hz, and (b) at 7500 Hz. The source is indicated by a filled black triangle and the nominal receiver depth is marked with a dashed black line. (c) Plot of TL (dB) as a function of range (km) averaged over the 6–7-m depth bins (nominal receiver depth was 6.5 m) for 2250 Hz (red line) and 7500 Hz (blue line).

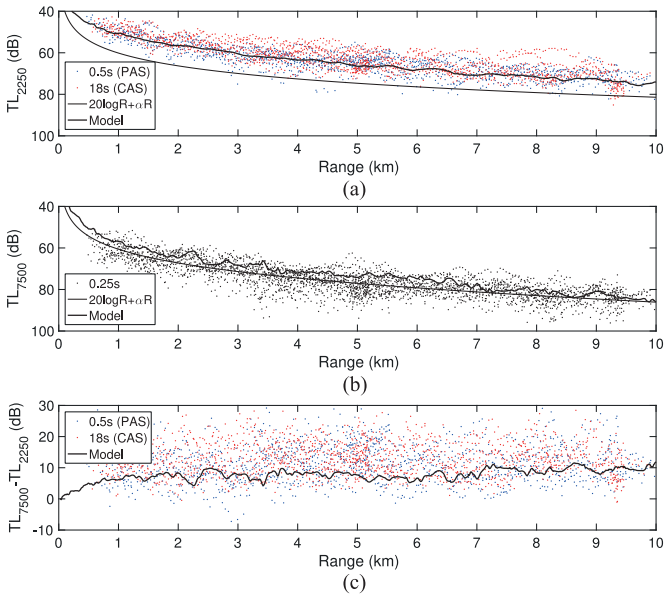

Fig. 6. TL as a function of range for runs on May 8–13, 2013, by frequency: (a) 2250 Hz, 0.5-s pulse/PAS (blue), 18-s pulse/CAS (red), $20 \log R + \alpha R$ (thin black line), model results (thick black line); (b) 7500 Hz, 0.25-s pulse (black), $20 \log R + \alpha R$ (thin black line), model results (thick black line); (c) difference $\mathrm{TL}_{7500} - \mathrm{TL}_{2250}$ calculated for each PAS (blue) or CAS (red) pulse, difference in model results (thick black line).

B. One-Way TL

1) Data Overview: Fig. 6 is a scatter plot of the measured TL for each pulse at 2250 Hz [see Fig. 6(a)] and 7500 Hz [see Fig. 6(b)] as a function of range, for all the pulses over the six-day period of May 8–13, 2013. Two theoretical TL curves are overlaid as a visual guide: The curve for spherical spreading loss with attenuation, and the curve calculated from model results. The spreading loss was calculated using $\mathrm{TL} = 20 \log R + \alpha_m R$, with R in meters, $\alpha_m = 1.41 \times 10^{-4}$ dB/m at 2250 Hz, and $\alpha_m = 6.10 \times 10^{-4}$ dB/m at 7500 Hz. The TL curve based on model results was averaged over both tracks and the 6–7 m depth bins.

The scatter in TL at any given range is large ($\pm$10 dB) and does not depend on range. The measured TL is less than spherical spreading at 2250 Hz and approximately equal to spherical spreading at 7500 Hz, while the Bellhop model TL is approximately centered on the measured data at 2250 Hz, but is smaller than most of the measured data at 7500 Hz. Looking at all the pulses grouped by frequency and pulse length, the mean difference and standard deviation were $\Delta\mathrm{TL}^{2250}_{\mathrm{model}} = -2.4 \pm 4.2$ dB for the 18-s CAS pulses, $\Delta\mathrm{TL}^{2250}_{\mathrm{model}} = -0.6 \pm 3.9$ dB for the 0.5-s PAS pulses, and $\Delta\mathrm{TL}^{7500}_{\mathrm{model}} = 2.9 \pm 5.1$ dB for the 0.25-s pulses. Although the mean values are within one standard deviation of zero, the measured TL is smaller than model predictions at 2250 Hz and larger than model predictions at 7500 Hz. Small-scale roughness either from waves or bottom roughness would tend to increase the relative loss of the higher frequency waveforms. Model estimates of loss due to bubbles could also be overestimated, as the surface loss model is predicated on a fully developed sea. Furthermore, at 2250 Hz the average CAS TL is 1.6 dB smaller than the average PAS TL, suggesting that the relative coherence loss (which is larger for the PAS pulses than the CAS pulses) reduces the TL in the PAS case.

Fig. 6(c) is a plot of the difference in TL between the two frequencies ($\mathrm{TL}_{7500} - \mathrm{TL}_{2250}$) for each pulse pair as a function of range. For both the CAS and the PAS runs, the TL difference has no range dependence [see Fig. 6(c)], with linear regression coefficients of less than 0.002 for both types of runs. The mean difference and standard deviation is 11.6 $\pm$ 6.0 dB for the CAS runs and 13.0 $\pm$ 5.5 dB for the PAS runs. The expected TL difference between frequencies [the black line in Fig. 6(c)] can be subtracted from each value of $\mathrm{TL}_{7500} - \mathrm{TL}_{2250}$, leaving an average of 5.2 $\pm$ 5.6 dB and 3.8 $\pm$ 6.3 dB of TL difference unexplained for CAS and PAS pulses, respectively. There is no way to determine whether the additional difference is due to the model overestimating the TL at 2250 Hz or underestimating the TL at 7500 Hz, or the sum of both systematic offsets.

2) Range-Binned TL: Fig. 7 contains plots of $\mathrm{TL}^{2250}_{\mathrm{mean}}$ as a function of range and grouped by day [see Fig. 7(a)–(e)]. Fig. 7(f) is a plot of $\mathrm{TL}^{2250}_{\mathrm{mean}}$ as a function of range for all pulses along each track, and for the entire data set. Dashed lines denote runs along the reverb track and solid lines denote runs along the clutter track. Sunrise and sunset times on May 10, the midpoint of the data set, were 05:52 L and 19:30 L (local time was Central Daylight Time). The TL plot lines are colored to indicate the time of day for each run: Blue for morning (sunrise—10:30), red for mid-day (10:30–15:00) and green for afternoon (15:00—sunset). The overall shapes of the TL curves are generally similar on any given day, with scatter as high as $\pm$5 dB from run to run. There is no consistent effect of time of day or pulse length (i.e.,

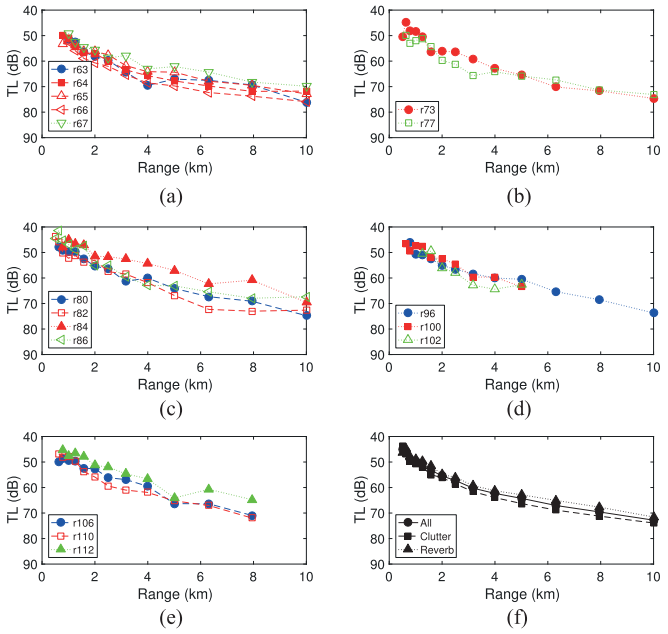

Fig. 7. Third-octave range-averaged TL (dB) as a function of range (km) for 18-s CAS and 0.5-s PAS pulses at 2250 Hz, with dotted lines indicating runs along the reverb track and dashed lines indicating runs along the clutter track. The plot colors indicate the time of day for the run: morning (blue), mid-day (red), or afternoon (green). Symbol fill indicates pulse type: CAS (filled) or PAS (hollow). Subplots (a) through (e) each contain the runs for a single day: (a) May 8, (b) May 9, (c) May 10, (d) May 12, (e) May 13, while (f) contains the average curve for each track as well as that for the combined data set of all TL measurements at 2250 Hz.

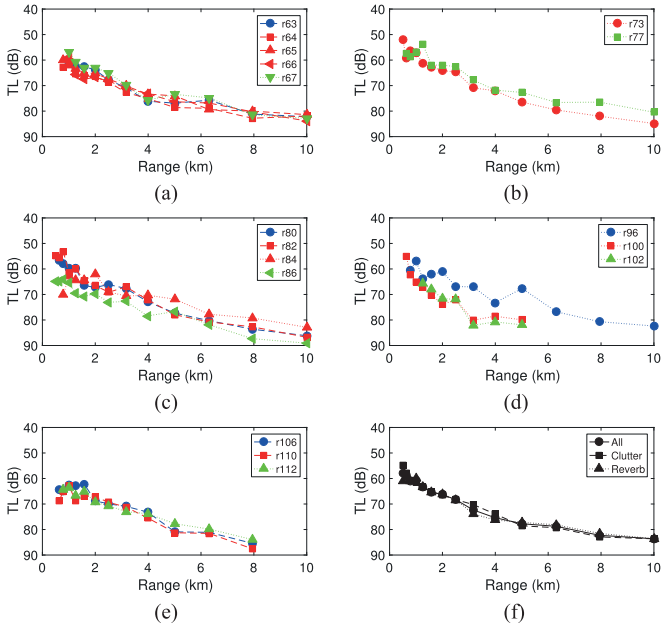

Fig. 8. Third-octave range-averaged TL (dB) as a function of range (km) for 0.25-s pulses at 7500 Hz, with dotted lines indicating runs along the reverb track and dashed lines indicating runs along the clutter track. The plot colors indicate the time of day for the run: morning (blue), mid-day (red), or afternoon (green). Subplots (a) through (e) each contain the runs for a single day: (a) May 8, (b) May 9, (c) May 10, (d) May 12, (e) May 13, while (f) contains the average curve for each track as well as that for the combined data set of all TL measurements at 7500 Hz.

PAS or CAS) on the TL. For ranges greater than 2 km, the TL along the clutter track is 4-dB higher than that on the reverb track [see Fig. 7(f)]. The TL difference between tracks is not consistent on individual runs; e.g., on May 10 [see Fig. 7(c)], the dotted green line (reverb track) is overlaid on the dashed blue line (clutter track) to ranges of 8 km.

Fig. 8 contains plots of $\mathrm{TL}_{\mathrm{mean}}^{7500}$ as a function of range and grouped by day, with the same plot arrangement and symbology as in Fig. 7. The TL curves at 7500 Hz are less smooth than those at 2250 Hz and the overall mean TL is 12 dB higher at 10 km range for 7500 Hz compared to 2250 Hz, consistent with model predictions [see Fig. 5(c)]. One noticeable feature is the higher loss (10–12 dB greater) at ranges beyond 2 km along the trombone runs on May 12 [see Fig. 8(d)], likely caused by changes in the depth of the towed receiver in response to the maneuvers of *CFAV Quest*. The mean TL curves on each track [see Fig. 8(f)] are within 3 dB of each other and there is no systematic difference between the two tracks as was seen at 2250 Hz.

3) Statistics: Recall (see Section II-B4) that one of the questions being explored is how to choose an appropriate central value about which the TL variability ($\Delta\mathrm{TL}$) is calculated, and furthermore, to explore whether the data are normally distributed about the central TL. Fig. 9(a) is a sample histogram calculated using the modeled TL as the central TL, while Fig. 9(b) is a histogram calculated using the mean TL as the central TL. According to the AD test results, the histogram in Fig. 9(a) is normally distributed, while Fig. 9(b) is not, with a level of significance $\alpha = 0.001$.

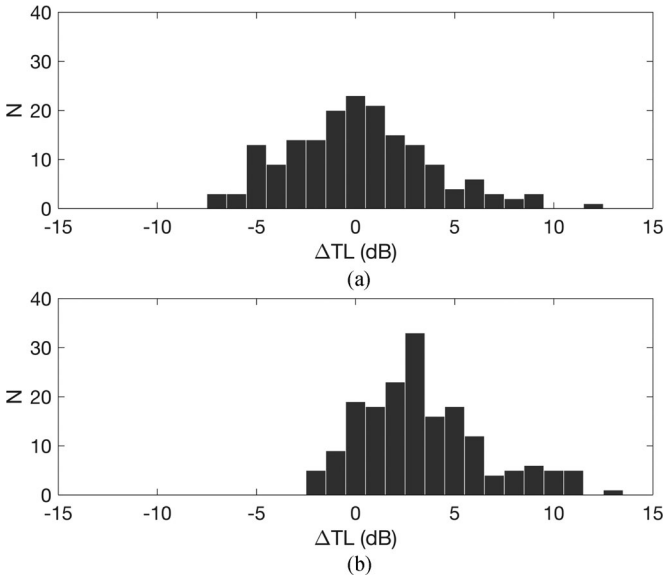

Fig. 9. Histograms of $\Delta\mathrm{TL}$ at 2250 Hz for run r77 using (a) model TL as the central value and (b) mean TL as the central value. The AD test results indicate that (b) is not normally distributed.

The AD test was run on all the TL data sets at both 2250 and 7500 Hz and using both types of TL (modeled and measured) as the central value. Fig. 10 is a plot of the mean and standard deviation in variability at 2250 Hz [see Fig. 10(a)] and 7500 Hz

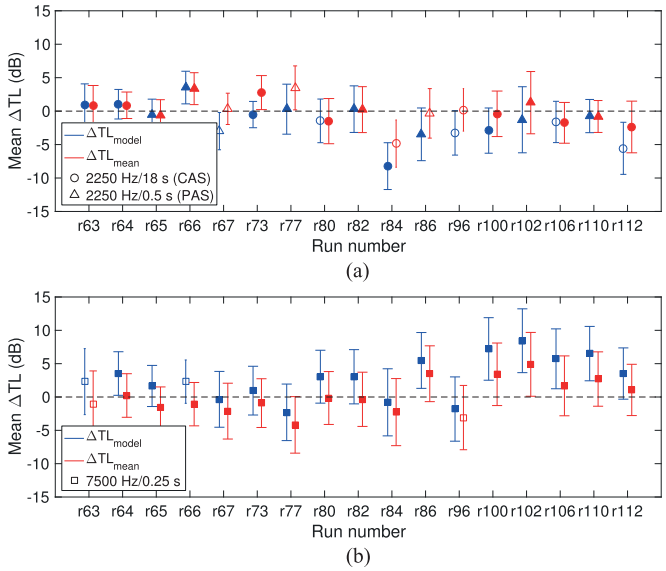

Fig. 10. Mean and standard deviation of variability by run for (a) $\Delta\mathrm{TL}^{2250}_{\mathrm{model}}$ (blue) and $\Delta\mathrm{TL}^{2250}_{\mathrm{mean}}$ (red) for CAS pulses (○) and PAS pulses (△), and (b) $\Delta\mathrm{TL}^{7500}_{\mathrm{model}}$ (blue) and $\Delta\mathrm{TL}^{7500}_{\mathrm{mean}}$ (red) (□). In both plots, color indicates the central TL used to calculate the variability (blue: model TL, red: mean TL). Symbol fill indicates the AD test results: normally distributed (filled) or not (hollow).

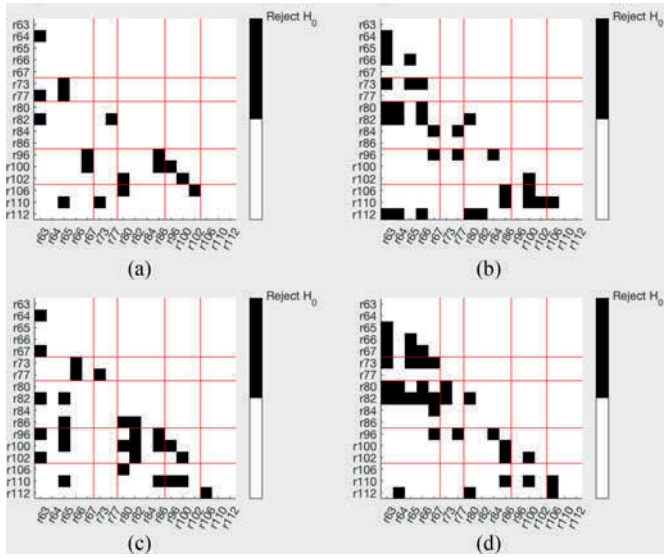

Fig. 11. Two-sample KS test results for pairs of runs: (a) $\Delta\mathrm{TL}^{2250}_{\mathrm{model}}$, (b) $\Delta\mathrm{TL}^{7500}_{\mathrm{model}}$, (c) $\Delta\mathrm{TL}^{2250}_{\mathrm{mean}}$, and (d) $\Delta\mathrm{TL}^{7500}_{\mathrm{mean}}$. Red lines separate the different days on which the data were acquired. Squares colored black indicate a rejection of H_0, that is, the observed values of $\Delta\mathrm{TL}$ were not drawn from the same distribution.

[see Fig. 10(b)] using both the modeled TL (blue symbols) and the mean measured TL (red symbols), with the results of the AD test for normality indicated by the symbol fill: The non-Gaussian distributions are plotted as hollow symbols. Most of the runs have a mean $\Delta\mathrm{TL}$ that is within one standard deviation of zero, regardless of the choice of central TL. According to the AD statistic, 5 of 17 runs at 2250 Hz and 2 of 17 runs at 7500 Hz were not normally distributed. Some runs (e.g., r67 at 2250 Hz) were not normally distributed about either the model or mean TL, while for other runs (e.g., r80 at 2250 Hz) the TL was normally distributed about the mean TL curve, but not the modeled TL curve. The mean $\Delta\mathrm{TL}$ relative to the model TL for all runs was -1.56 dB at 2250 Hz and 2.85 dB at 7500 Hz, indicating that the model was overestimating loss at 2250 Hz and underestimating TL at 7500 Hz. The mean standard deviations for all runs were 3.2 dB ($\Delta\mathrm{TL}^{2250}_{\mathrm{model}}$), 4.2 dB ($\Delta\mathrm{TL}^{7500}_{\mathrm{model}}$), 3.1 dB ($\Delta\mathrm{TL}^{2250}_{\mathrm{mean}}$), and 3.7 dB ($\Delta\mathrm{TL}^{7500}_{\mathrm{mean}}$). It is interesting that the standard deviations fell in a narrow range of 3.2–4.2 dB regardless of the TL chosen for comparison, though they were slightly higher at 7500 Hz (3.7–4.2 dB) than 2250 Hz (3.1–3.2 dB).

Variability was explored in with respect to both time and frequency. First, on each run, the TL variability at the two frequencies (2250 and 7500 Hz) was compared using the KS test to determine whether the observed $\Delta\mathrm{TL}$ values were likely drawn from the same distributions. Second, the KS test was used on each pairwise combination of runs, to determine whether the observed $\Delta\mathrm{TL}$ values from different dates and times were likely drawn from the same distributions.

For the first test, pairing up $\Delta\mathrm{TL}$ values at different frequencies on the same run, only runs r80 and r82 resulted in a rejection of H_0, and the same result was obtained when using either the model TL or mean TL was used as the central TL. That is, the observed values of $\Delta\mathrm{TL}$ were not likely drawn from the same distribution at both 2250 and 7500 Hz for only 2 of 17 runs.

For the second test, pairing up $\Delta\mathrm{TL}$ at the same frequencies on different runs, the results are displayed graphically in Fig. 11; a black square indicates that H_0 was rejected (i.e., $\Delta\mathrm{TL}$ was not drawn from the same distribution) for the pairing of runs indicated by the intersection of the row and columns. Fig. 11(a) and (b) shows the comparisons for $\Delta\mathrm{TL}^{2250}_{\mathrm{model}}$ and $\Delta\mathrm{TL}^{7500}_{\mathrm{model}}$ while Fig. 11(c) and (d) shows the comparisons for $\Delta\mathrm{TL}^{2250}_{\mathrm{mean}}$ and $\Delta\mathrm{TL}^{7500}_{\mathrm{mean}}$. Most of the squares are white, indicating that in most cases $\Delta\mathrm{TL}$ was drawn from the same distribution; however, when using the mean TL curve as the central TL [see Fig. 11(c) and (d)], H_0 was rejected slightly more often (21% and 25% of the pairings at 2250 and 7500 Hz) than when using the model TL curve as the central TL (Fig. 11(a) and b, 13% and 23% of the pairings at 2250 and 7500 Hz).

C. Two-Way TL

Using the echo-repeated signal, comparisons were made of the original and echo-repeated TL (TL_1 and TL_2, respectively) for the subset of runs with the highest target strength setting (25 dB) and therefore the highest signal-to-noise ratio, which were the runs on May 8 and 9 (r63, r64, r65, r67, r73, and r77). Recall that only the 2250-Hz CAS or PAS pulses were echo-repeated, and the echo-repeat was transmitted in one of two configurations: Either ping pong mode, in which the 2250-Hz original pulse was recorded and echo-repeated 20 s later during the next pulse; or dual band mode, in which an out-of-band

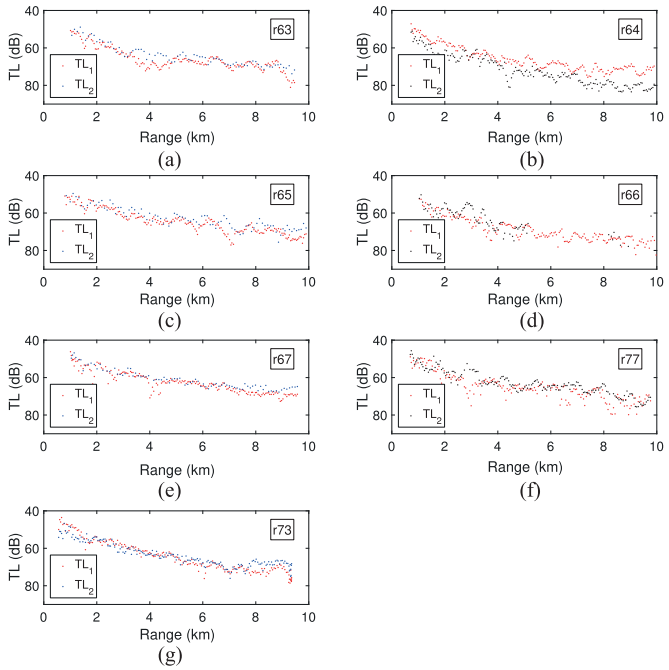

Fig. 12. TL (dB) as a function of range (km) for original pulses (TL_1) and echo-repeated pulses (TL_2) for runs on May 8 and 9. The plots in the left column are for the ping pong runs (a) r63, (c) r65, (e) r67, and (g) r73, and the plots in the right column are for the dual band runs (b) r64, (d) r65, and (f) r77.

pulse centered at 3750 Hz was recorded and retransmitted within 500 ms at a reduced sampling rate equivalent to the 2250-Hz pulse.

In a "frozen" ocean with colocated sources and receivers, the two one-way transmission losses TL_1 and TL_2 should be equal. For the echo-repeat experiments the colocated source and receiver geometry is not quite achieved, as the echo-repeat source is 3.5-m deeper than the LAMDA array receiver, and their range separation is 75 m. Furthermore, on the ping pong mode runs, the ship moves 40–50 m during the 20-s time between the original pulse and the echo-repeated pulse.

Fig. 12 is a plot of TL_1 and TL_2 as a function of range, arranged with the ping pong runs on the left [see Fig. 12(a), (c), (e), and (g)] and the dual band runs on the right [see Fig. 12(b), (d), and (f)]. For the dual band runs, the TL_1 and TL_2 measurements have very different features: Systematic offsets [see Fig. 12(b)], as well as probable nulls and caustics appearing at different ranges for TL_1 than for TL_2 [see Fig. 12(b), (d), and (f)]. It is possible that the dual band transmissions did not actually occur over reciprocal paths. Also, the frequency-dependent scattering and losses distorted the dual band signal significantly, and this distortion was subsequently amplified and retransmitted at different frequencies than the original signal during the echo-repeat process.

Given the apparent instability of the dual band echo repeat process, the statistical properties of the difference $\Delta\mathrm{TL}= \mathrm{TL}_1 - \mathrm{TL}_2$ were examined only for the four ping pong runs in Fig. 12. For the ping pong runs, the values of $\Delta\mathrm{TL}$ were normally distributed according to the AD test. For each run, the mean value of $\Delta\mathrm{TL}$ was within one standard deviation of zero, and the mean standard deviation in $\Delta\mathrm{TL}$ across all four ping pong runs was 2.82 dB. For the KS test, there are six possible pairings of the four ping pong runs; all but one pairing (r65 and r73) were drawn from the same distribution. In light of the KS test results, and after examining the plots of the ping pong TL data in Fig. 12, it is possible that the nonreciprocal paths were also a problem for the ping pong runs, in particular r63 and r65. Therefore, even with the relatively small spatial deviation from true reciprocity (75 m horizontally and 3.5 m in depth), it appears to be unreasonable to compare TL_1 to TL_2 for the geometry and pulse types used in this particular experiment.

IV. Conclusion

TL variability was examined on a variety of time scales for three LFM waveform types: 2250-Hz 18-s pulses (900-Hz bandwidth), 2250-Hz 0.5-s pulses (900-Hz bandwidth), and 7500-Hz 0.25 s pulses (1000-Hz bandwidth).

Two possibilities were examined for the choice of central TL about which to measure the variability $\Delta\mathrm{TL}$: A mean value and a modeled value. The mean TL curve was calculated from the measured TL along each of two tracks by combining the data into third-octave range bins. The modeled TL value was calculated using measured bathymetry for each track, the mean sound-speed profile, and representative range-independent bottom properties. The TL data were tested for deviations from a normal distribution about each type of central TL. In most cases (65%–94% of the runs) the data were normally distributed regardless of whether the modeled or measured TL was used for comparison, and most of the runs (71%–88%) had mean values of $\Delta\mathrm{TL}$ that lay within one standard deviation of zero. In addition, statistical tests support the null hypothesis that most of the TL data (75%–82% of possible pairings of data sets) were drawn from the same underlying statistical distribution regardless of central TL, pulse length, and frequency.

TL variability ($\Delta\mathrm{TL}$) was examined by calculating the difference between the observed TL for the ith measurement TL_i and the central TL value (i.e., $\Delta\mathrm{TL}_{\mathrm{mean}} = \mathrm{TL}_{\mathrm{mean}} - \mathrm{TL}_i$ and $\Delta\mathrm{TL}_{\mathrm{model}} = \mathrm{TL}_{\mathrm{model}} - \mathrm{TL}_i$). The variability was investigated at a variety of time scales: Milliseconds, tens of seconds, one hour, one day, and six days. Over the shortest time scale studied, which was the 250 ms between the 7500-Hz trigger pulse and the 2250-Hz main pulse, the variability was 5–6 dB after accounting for the frequency-dependent offset. The two-way TL could have given some insight into the variability over the 20 s between pulses; however, the propagation paths were not truly reciprocal and therefore comparisons between TL_1 and TL_2 were not as useful as was hoped. During a 1-h run, the variability was consistently ± 4 dB, while over the timescale of several hours from run to run, the variability was ± 5 dB. Over the course of the entire six-day period, the variability was as large as ± 10 dB for TL measurements at the same source–receiver range.

The data were examined for effects of pulse length, bathymetry, and bottom properties, and time of day. The TL was,

on average, 1.6 dB lower for CAS pulses than for PAS pulses, likely due to the larger relative coherence loss for the shorter PAS pulses. The differing bathymetry and bottom composition on the reverb and clutter tracks resulted in a difference in TL at 2250 Hz, but not at 7500 Hz. However, the observed 4-dB increase in TL on the clutter track compared to the reverb track was only observed when averaging over the entire six-day data set; consistent differences were not observed on individual runs, suggesting that the shorter timescale changes in the water column dominated the observed TL curve for any particular run and obscured the effects of the bathymetry and bottom composition. The time of day did not have any consistent effect on the observed TL, in spite of the change from isospeed conditions overnight to downward-refracting over the course of the day.

The very shallow water, mid-frequency study considered in this paper is likely influenced more by boundary interactions than earlier studies, therefore it is not surprising that the observed variability is higher. The fact that the TL variability was normally distributed regardless of choice of central TL implies that, in the absence of extensive TL measurements for a particular operational area, it should be possible to provide reliable sonar performance predictions based on propagation model calculations using representative environmental inputs. Furthermore, the data presented here suggest that it is reasonable to assume Gaussian statistics for TL variability when calculating probabilities of detection at frequencies common in modern anti-submarine warfare applications. Ideally, there should be a connection between the timescales of dominant underlying oceanographic processes and the magnitude of TL variability over comparable timescales; however, the data set from TREX13 did not allow for such correlations to be made.

ACKNOWLEDGMENT

The authors would like to thank Dr. P. Hines, J. Scrutton, and S. Murphy of DRDC Atlantic for planning the TREX13 experiments; Dr. D. Tang, Dr. T. Hefner, and Dr. K. Williams of APL-UW who managed and led the TREX13 trial; B. Brand of APL-UW who managed acoustic transmissions; and Dr. J. Preston of the Applied Research Laboratory at the Pennsylvania State University who managed quality control and data collection for the experiment. The authors would also like to thank the contribution of the technical staff at DRDC Atlantic, the officers and crew aboard *CFAV Quest* and *R/V Sharp*, and the APL-UW dive team for their support throughout the trial. Finally, the authors would like to thank Dr. D. Dall'Osto and Dr. P. Dahl of APL-UW for providing the data from the wave buoy.

REFERENCES

[1] C. Eckart and R. Carhart, "Fluctuations of sound in the sea," in *National Research Council Committee on Undersea Warfare, Panel on Underwater Acoustics*. A Survey Report on Basic Problems of Underwater Acoustics Research, Washington, D. C., National Research Council, pp. 63–121, 1950.

[2] N. G. Pace and F. B. Jensen, Eds., *Impact of Littoral Environmental Variability on Acoustic Predictions and Sonar Performance*. Dordrecht, The Netherlands: Kluwer, 2002, ch. 1–4.

[3] J. Potter and A. Warn-Varnas, *Ocean Variability & Acoustic Propagation*. Dordrecht, The Netherlands: Springer Netherlands, 2012.

[4] K. LePage, "Modeling propagation and reverberation sensitivity to oceanographic and seabed variability," *IEEE J. Ocean. Eng.*, vol. 31, no. 2, pp. 402–412, Apr. 2006.

[5] E. I. Thorsos, F. S. Henyey, K. L. Williams, W. T. Elam, and S. A. Reynolds, "Simulations of temporal and spatial variability in shallow water propagation," in *Impact of Littoral Environmental Variability on Acoustic Predictions and Sonar Performance*, N. G. Pace and F. B. Jensen, Eds. Dordrecht, The Netherlands: Kluwer, 2002, pp. 337–344.

[6] L. Sha and L. W. Nolte, "Effects of environmental uncertainties on sonar detection performance prediction," *J. Acoust. Soc. Amer.*, vol. 117, pp. 1942–1953, 2004.

[7] K. D. LePage, C. Holland, and J. A. Goff, "Transfer of oceanographic and bottom variability into shallow water propagation and reverberation uncertainty," *J. Acoust. Soc. Amer.*, vol. 114, pp. 2311–2312, 2003.

[8] R. T. Kessel, "A mode-based measure of field sensitivity to geoacoustic parameters in weakly range-dependent environments," *J. Acoust. Soc. Amer.*, vol. 105, pp. 122–123, 1999.

[9] S. E. Dosso, P. M. Giles, G. H. Brooke, D. F. McCammon, S. P. Pecknold, and P. C. Hines, "Linear and nonlinear measures of ocean acoustic environmental sensitivity," *J. Acoust. Soc. Amer.*, vol. 121, no. 1, pp. 42–45, 2007.

[10] S. P. Pecknold, K. W. Masui, and P. C. Hines, "Transmission loss measurements and geoacoustic sensitivity modeling at 1.2 kHz," *J. Acoust. Soc. Amer.*, vol. 124, no. 3, pp. EL110–EL115, 2008.

[11] S. P. Pecknold and J. C. Osler, "Sensitivity of acoustic propagation to uncertainties in the marine environment as characterized by various rapid environmental assessment methods," *Ocean Dyn.*, vol. 62, no. 2, pp. 265–281, 2012.

[12] C. Emerson *et al.*, "Acoustic propagation uncertainty and probabilistic prediction of sonar system performance in the southern East China Sea continental shelf and shelfbreak environments," *IEEE J. Ocean. Eng.*, vol. 40, no. 4, pp. 1003–1017, Oct. 2015.

[13] B. H. Pasewar, S. N. Wolf, M. H. Orr, and J. F. Lynch, "Acoustic intensity variability in a shallow water environment," in *Impact of Littoral Environmental Variability on Acoustic Predictions and Sonar Performance*, N. G. Pace and F. B. Jensen, Eds. Dordrecht, The Netherlands: Kluwer, 2002, pp. 337–344.

[14] D. F. McCammon, "Users guide to BellhopDRDC_active_v5: Active v5 and updated passive v4a," McCammon Acoustical Consulting, DRDC Atlantic, Ottawa, ON, Canada, Rep. CR 2010-319, 2011.

[15] P. C. Hines, S. M. Murphy, D. A. Abraham, and G. B. Deane, "The dependence of signal coherence on sea-surface roughness for high and low duty cycle sonars in a shallow-water channel," *IEEE J. Ocean. Eng.*, vol. 42, no. 2, pp. 298–318, Apr. 2017.

[16] S. Murphy, J. G. E. Scrutton, and P. C. Hines, "Experimental implementation of an echo repeater for continuous active sonar," *IEEE J. Ocean. Eng.*, vol. 42, no. 2, pp. 289–297, Apr. 2017.

[17] J. Preston, K. Becker, P. Shultz, and J. McIlvain, "An overview and lessons learned from the Five Octave Research Array (FORA) and some perspectives for future towed arrays," in *Proc. 4th Int. Conf. Underwater Acoust. Meas., Technol. Results*, Kos, Greece, 2011, pp. 1241–1248.

[18] P. H. Dahl, and D. R. Dall'Osto, "Observations of sea-surface waves during the 2013 target and reverberation experiment (TREX13) and relation to midfrequency sonar," *IEEE J. Ocean. Eng.*, vol. 42, no. 2, pp. 250–259, Apr. 2017.

[19] M. B. Porter and H. P. Bucker, "Gaussian beam tracing for computing ocean acoustic fields," *J. Acoust. Soc. Amer.*, vol. 82, no. 4, pp. 1349–1359, 1987.

[20] S. P. Pecknold, J. A. Theriault, D. McGaughey, and J. Collins, "Time-series modeling using the waveform transmission through a channel program," in *Proc. OCEANS Conf.*, 2005, pp. 1–8.

[21] P. Abbot and I. Dyer, "Sonar performance predictions incorporating environmental variability," in *Impact of Littoral Environmental Variability of Acoustic Predictions and Sonar Performance*. Dordrecht, The Netherlands: Springer-Verlag, 2002, pp. 611–618.

[22] T. W. Anderson and D. A. Darling, "A test of goodness of fit," *J. Amer. Stat. Assoc.*, vol. 49, no. 268, pp. 765–769, 1954.

[23] N. M. Razali and Y. B. Wah, "Power comparisons of Shapiro–Wilk, Kolmogorov–Smirnov, Lilliefors and Anderson–Darling tests," *J. Stat. Model. Anal.*, vol. 2, no. 1, pp. 21–33, 2011.

[24] W. H. Press, *Numerical Recipes: The Art of Scientific Computing*, 2nd ed. Cambridge, U.K.: Cambridge Univ. Press, 1992, ch. 14.

[25] F. J. Massey, Jr., "The Kolmogorov-Smirnov test for goodness of fit," *J. Amer. Stat. Assoc.*, vol. 46, no. 253, pp. 68–78, 1951.

Cristina D. S. Tollefsen received the B.Sc. and M.Sc. degrees in physics from the University of Manitoba, Winnipeg, MB, Canada, in 1998 and 2000, respectively, and the Ph.D. degree in physical oceanography from Memorial University of Newfoundland, St. John's, NL, Canada, in 2005.

She is currently a Defence Scientist in the Underwater Sensing Section, Defence Research and Development Canada's Atlantic Research Centre, Dartmouth, NS, Canada. Her current research interests include effects of physical oceanographic processes on acoustical propagation, and multistatic sonar performance modeling.

Dr. Tollefsen is a member of the Acoustical Society of America.

Sean P. Pecknold received the Ph.D. degree in physics from McGill University, Montreal, QC, Canada, in 2000.

He is currently a Defence Scientist in the Underwater Sensing Section, Defence Research and Development Canada's Atlantic Research Centre, Dartmouth, NS, Canada, where his research interests include acoustical propagation uncertainty and geoacoustic parameter estimation.

Dr. Pecknold is a member of the Canadian Acoustical Association and the Acoustical Society of America.

DOCUMENT CONTROL DATA

(Security markings for the title, abstract and indexing annotation must be entered when the document is Classified or Designated)

1. ORIGINATOR (The name and address of the organization preparing the document. Organizations for whom the document was prepared, e.g., Centre sponsoring a contractor's report, or tasking agency, are entered in Section 8.)

DRDC – Atlantic Research Centre
Defence Research and Development Canada
9 Grove Street
P.O. Box 1012
Dartmouth, Nova Scotia B2Y 3Z7
Canada

2a. SECURITY MARKING (Overall security marking of the document including special supplemental markings if applicable.)

CAN UNCLASSIFIED

2b. CONTROLLED GOODS

NON-CONTROLLED GOODS
DMC A

3. TITLE (The complete document title as indicated on the title page. Its classification should be indicated by the appropriate abbreviation (S, C or U) in parentheses after the title.)

Characterizing Transmission Loss Variability During the Target and Reverberation Experiment 2013

4. AUTHORS (last name, followed by initials – ranks, titles, etc., not to be used)

Tollefsen, C.D.S.; Pecknold, S.P.

5. DATE OF PUBLICATION (Month and year of publication of document.)	6a. NO. OF PAGES (Total containing information, including Annexes, Appendices, etc.)	6b. NO. OF REFS (Total cited in document.)
October 2017	11	25

7. DESCRIPTIVE NOTES (The category of the document, e.g., technical report, technical note or memorandum. If appropriate, enter the type of report, e.g., interim, progress, summary, annual or final. Give the inclusive dates when a specific reporting period is covered.)

External Literature (P)

8. SPONSORING ACTIVITY (The name of the department project office or laboratory sponsoring the research and development – include address.)

DRDC – Atlantic Research Centre
Defence Research and Development Canada
9 Grove Street
P.O. Box 1012
Dartmouth, Nova Scotia B2Y 3Z7
Canada

9a. PROJECT OR GRANT NO. (If appropriate, the applicable research and development project or grant number under which the document was written. Please specify whether project or grant.)	9b. CONTRACT NO. (If appropriate, the applicable number under which the document was written.)

10a. ORIGINATOR'S DOCUMENT NUMBER (The official document number by which the document is identified by the originating activity. This number must be unique to this document.)	10b. OTHER DOCUMENT NO(s). (Any other numbers which may be assigned this document either by the originator or by the sponsor.)
DRDC-RDDC-2017-P085	

11a. FUTURE DISTRIBUTION (Any limitations on further dissemination of the document, other than those imposed by security classification.)

Public release

11b. FUTURE DISTRIBUTION OUTSIDE CANADA (Any limitations on further dissemination of the document, other than those imposed by security classification.)

12. ABSTRACT (A brief and factual summary of the document. It may also appear elsewhere in the body of the document itself. It is highly desirable that the abstract of classified documents be unclassified. Each paragraph of the abstract shall begin with an indication of the security classification of the information in the paragraph (unless the document itself is unclassified) represented as (S), (C), (R), or (U). It is not necessary to include here abstracts in both official languages unless the text is bilingual.)

A significant driver of uncertainty in sonar performance is the variability in underwater acoustical propagation caused by environmental fluctuations and uncertainty in the position of sources, targets, and receivers. A set of echo-repeat experiments was conducted during the Target and Reverberation Experiment 2013 (TREX13), a sea trial that took place in April to May 2013 in the Gulf of Mexico near Panama City, FL, USA. The variability in measured transmission loss (TL) was characterized using two different methods: Variability with respect to a mean observed TL, and variability with respect to modeled TL. Both one-way and quasi-reciprocal two-way TL measurements at 2250 and 7500 Hz were analyzed to characterize the variability at timescales ranging from less than one second to several days, with the results indicating that the acoustic propagation fluctuates stochastically on all these time scales. The results of statistical tests suggest that the TL variability can be treated as Gaussian fluctuations about a central TL obtained from an acoustic propagation model, with standard deviations of 5 dB over timescales up to one day, or 10 dB over timescales from one to six days.

13. KEYWORDS, DESCRIPTORS or IDENTIFIERS (Technically meaningful terms or short phrases that characterize a document and could be helpful in cataloguing the document. They should be selected so that no security classification is required. Identifiers, such as equipment model designation, trade name, military project code name, geographic location may also be included. If possible keywords should be selected from a published thesaurus, e.g., Thesaurus of Engineering and Scientific Terms (TEST) and that thesaurus identified. If it is not possible to select indexing terms which are Unclassified, the classification of each should be indicated as with the title.)

Underwater acoustics; acoustic propagation